Analytical model of the deformation-induced inertial dynamics of a magnetic vortex

Myoung-Woo Yoo, Francesca Mineo, Joo-Von Kim

Journal of Applied Physics ARTICLE scitation.org/journal/jap

Analytical model of the deformation-induced inertial dynamics of a magnetic vortex

Cite as: J. Appl. Phys. **129**, 053903 (2021); doi: 10.1063/5.0039535
Submitted: 3 December 2020 · Accepted: 9 January 2021 ·
Published Online: 4 February 2021

Myoung-Woo Yoo,[1,2,a)] Francesca Mineo,[1,3,4] and Joo-Von Kim[1]

AFFILIATIONS

[1]Centre de Nanosciences et de Nanotechnologies, CNRS, Université Paris-Saclay, 91120 Palaiseau, France
[2]Chaire Photonique, Laboratoire Matériaux Optiques, Photonique et Systèmes, CentraleSupélec, Université de Lorraine, 57070 Metz, France
[3]Max Planck Institute for the Science of Light, Staudtstraße 2, 91058 Erlangen, Germany
[4]Department of Physics, Friedrich-Alexander-Universität Erlangen-Nürnberg, 91058 Erlangen, Germany

[a)]**Author to whom correspondence should be addressed:** myoungwoo.yoo@gmail.com

ABSTRACT

We present an analytical model to account for the deformation-induced inertial dynamics of a magnetic vortex. The model is based on a deformation of the vortex core profile based on the Döring kinetic field, whereby the deformation amplitudes are promoted to dynamical variables in a collective-coordinate approach that provides a natural extension to the Thiele model. This extended model describes complex transients due to inertial effects and the variation of the effective mass with velocity. The model also provides a quantitative description of the inertial dynamics leading up to vortex core reversal, which is analogous to the Walker transition in domain wall dynamics. Our work paves the way for a standard prescription for describing the inertial effects of topological magnetic solitons.

I. INTRODUCTION

Topological solitons represent compact, nontrivial solutions of a nonlinear field system. In magnetic thin films, examples of such excitations include one-dimensional (1D) configurations like domain walls[1,2] and two-dimensional structures such as vortices[3–6] and skyrmions.[7,8] For the latter, a common approach for describing their dynamics involves a collective coordinates approach in which the position $\mathbf{X} = (X, Y)$ of the vortex or skyrmion core, assumed to be rigid, is elevated to a dynamical variable $\mathbf{X}(t)$ and subsequently defines the entire dynamics of the system by allowing all other degrees of freedom to be integrated out. This is the basis of the Thiele model,[4,9,10]

$$\mathbf{G} \times \dot{\mathbf{X}} + \alpha \overleftrightarrow{D} \cdot \dot{\mathbf{X}} = -\frac{\partial U}{\partial \mathbf{X}}, \tag{1}$$

where $\mathbf{G} = (M_s/\gamma) \int dV \sin\theta \, (\nabla\theta \times \nabla\phi)$ is the gyrovector, $\overleftrightarrow{D} = (M_s/\gamma) \int dV [\nabla\theta \otimes \nabla\theta + \sin^2\theta \, (\nabla\phi \otimes \nabla\phi)]$ is the damping tensor, α is the Gilbert constant, U is a total magnetic energy, M_s is the saturation magnetization, and γ is the gyromagnetic constant. Here, θ and ϕ represent the orientation of the magnetization field, $\mathbf{m}$, in spherical coordinates.

However, it has been known since the seminal work of Döring[11] that soliton motion in ferromagnetic materials should be accompanied by a deformation of the static configuration, since the Landau–Lifshitz equation governing the magnetization dynamics does not exhibit Galilean invariance and so changes to the static profile must appear for a soliton propagating at finite velocity in the steady state. This is apparent in the 1D model of domain wall dynamics, where in addition to the wall position $q(t)$ an additional dynamical variable, the *wall angle* $\varphi(t)$ appears in the equations of motion and describes a transformation from the equilibrium static wall profile.[12,13] In addition, the potential energy related to $\varphi(t)$ characterizes the wall mass and limits the propagation speed of the time-independent profile, a phenomenon known as Walker breakdown.

Magnetic vortex and skyrmion dynamics also have been studied extensively over the past few decades, such as translational motion,[9,10,14,15] the inertial effects,[16,17] core deformation and polarity switching,[18–21] and their internal eigenmodes.[22–26] Interestingly, despite the large body of theoretical work on such dynamics to date, a consistent description of inertial effects and

core deformation within the Thiele framework remains largely unexplored. Some earlier work has identified the importance of coupling to the spin waves as a source of inertia.[16,27–30] From a phenomenological standpoint, inertia can be introduced through the addition of a mass term $\mathcal{M}$,[17,27,31–35]

$$\mathcal{M}\ddot{\mathbf{X}} + \mathbf{G}\times\dot{\mathbf{X}} + \alpha\overleftrightarrow{D}\cdot\dot{\mathbf{X}} = -\frac{\partial U}{\partial \mathbf{X}}. \tag{2}$$

However, this approach neglects the change in internal energy as a result of changes to the magnetic configuration of the core, which occurs in processes such as vortex core reversal[19,36–38] and trochoidal motion of antiskyrmions,[39] which are phenomena analogous to Walker breakdown.

In this paper, we present a model to account for the motion-induced inertia of magnetic vortices. The remainder of the paper is organized as follows. In Sec. II, we describe the analytical approach for the deformation based on Döring's kinetic field and then derive equations of motion of the vortex core, from which the inertial motion can be described. Section III discusses in more detail the transient inertial dynamics that follows from the model, where comparisons with micromagnetic simulations show that features such as excitation of higher-order spin-wave modes can be accounted for. In Sec. IV, we show how the inertial mass depends on the core velocity. This is followed by a discussion on how inertial effects affect vortex core reversal in Sec. V. Last, a discussion and concluding remarks are presented in Sec. VI.

II. MODEL

Consider a moving vortex with a finite velocity, $\dot{\mathbf{X}}$. Under this steady motion, the magnetic configuration becomes deformed with respect to its static equilibrium state, which can be accounted for by minimizing the micromagnetic energy with respect to an additional "kinetic field" of the form, $\mathbf{H}_{\rm kin} = (1/\gamma_0)\mathbf{m}\times[(\dot{\mathbf{X}}\cdot\nabla)\mathbf{m}]$, where $\gamma_0 = \mu_0\gamma$ and $\mathbf{m} = (\sin\theta\cos\phi,\ \sin\theta\sin\phi,\ \cos\theta)$ is a unit vector of a local magnetic moment.[11,37,38] Let us assume that deformations $\delta\mathbf{m}$ to the static profile, $\mathbf{m}_0$, can be expressed in terms of a rotation of the magnetic moments toward the direction of the kinetic field under a small deformation, i.e., $\delta\mathbf{m} \propto -\mathbf{m}_0\times(\mathbf{m}_0\times\mathbf{H}_{\rm kin})$.[21,38] This leads to the deformation *ansatz*,

$$\theta(\mathbf{x},\boldsymbol{\xi}) = \theta_0 - \sin\theta_0[\boldsymbol{\xi}\cdot\nabla\phi_0], \tag{3a}$$

$$\phi(\mathbf{x},\boldsymbol{\xi}) = \phi_0 + \frac{1}{\sin\theta_0}[\boldsymbol{\xi}\cdot\nabla\theta_0], \tag{3b}$$

where $\theta_0 = \theta_0(\mathbf{x}-\mathbf{X})$ and $\phi_0 = \phi_0(\mathbf{x}-\mathbf{X})$ are the polar and azimuthal angles of the static configuration. $\boldsymbol{\xi}(t) = [\xi_x(t), \xi_y(t)]$ is a new dynamical variable that describes the deformation amplitude with dimensions of length. By using Eq. (3), we obtain the deformed configuration from the initial vortex state as presented in Fig. 1(a) in the case of a permalloy disk with a diameter of 512 nm and a thickness of 20 nm. The result shows that Eq. (3) gives a good description of the changes to the core profile as a result of its motion when compared with the simulated result [Fig. 1(b)], in particular, the asymmetric dip near the core center.[18–20] Note that Eq. (3) has a singularity at the center of the vortex core at which $\theta = 0$ or π.

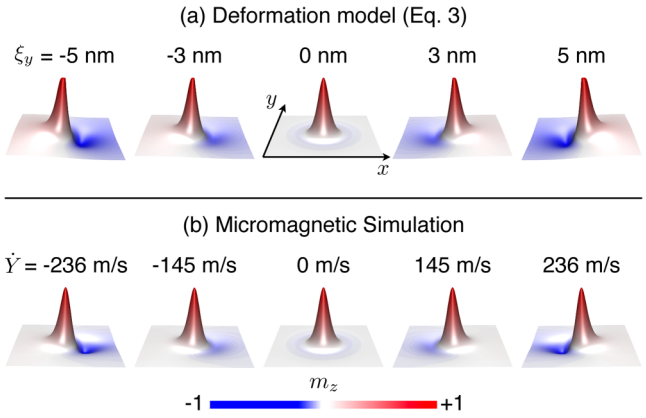

FIG. 1. (a) Deformed-vortex configurations near the core ($60\times60\,\mathrm{nm}^2$) calculated from the static configuration ($\xi_x = 0\,\mathrm{nm}$) using Eq. (3) with $\xi_x = -5, -3, 3$, and 5 nm. The height is proportional to m_z and the color indicates m_z as noted by the color bar. (b) Deformation of the vortex obtained from a micromagnetic simulation at the indicated velocity, $\dot{Y}$.

From Eq. (3), we can calculate the Euler–Lagrange equation,[12,40–42]

$$\frac{d}{dt}\frac{\partial L}{\partial\dot{q}} - \frac{\partial L}{\partial q} + \frac{\partial W}{\partial\dot{q}} = 0, \tag{4}$$

where $q = \{X, Y, \xi_x, \xi_y\}$ represent the generalized coordinates and

$$\begin{aligned} L &= \frac{M_s}{\gamma}\dot{\phi}(1-\cos\theta) - U,\\ W &= \alpha\frac{M_s}{2\gamma}\left[\left(\frac{d\theta}{dt}\right)^2 + \sin^2\theta\left(\frac{d\phi}{dt}\right)^2\right], \end{aligned} \tag{5}$$

are the Lagrangian and dissipative function densities, respectively. By solving the Euler–Lagrange equation and integrating over the volume, equations of motion can be derived with the four independent collective coordinates, X, Y, ξ_x, and ξ_y,

$$\mathbf{G}\times\left(\dot{\mathbf{X}} - \alpha\dot{\boldsymbol{\xi}}\right) + \overleftrightarrow{D}\cdot\left(\alpha\dot{\mathbf{X}} + \dot{\boldsymbol{\xi}}\right) = -\frac{\partial U}{\partial\mathbf{X}}, \tag{6a}$$

$$\mathbf{G}\times\left(\dot{\boldsymbol{\xi}} + \alpha\dot{\mathbf{X}}\right) + \overleftrightarrow{D}\cdot\left(\alpha\dot{\boldsymbol{\xi}} - \dot{\mathbf{X}}\right) = -\frac{\partial U}{\partial\boldsymbol{\xi}}. \tag{6b}$$

Here, $\mathbf{G} = G\hat{\mathbf{z}}$ and $\overleftrightarrow{D} = D\overleftrightarrow{I}$, where $\overleftrightarrow{I}$ is the 2×2 identity matrix and

$$\begin{aligned} G &= \frac{M_s}{\gamma}\int dV\sin\theta_0\left(\frac{\partial\theta_0}{\partial x}\frac{\partial\phi_0}{\partial y} - \frac{\partial\phi_0}{\partial y}\frac{\partial\theta_0}{\partial x}\right),\\ D &= \frac{M_s}{\gamma}\int dV\left(\left(\frac{\partial\theta_0}{\partial x}\right)^2 + \sin^2\theta_0\left(\frac{\partial\phi_0}{\partial x}\right)^2\right)\\ &= \frac{M_s}{\gamma}\int dV\left(\left(\frac{\partial\theta_0}{\partial y}\right)^2 + \sin^2\theta_0\left(\frac{\partial\phi_0}{\partial y}\right)^2\right). \end{aligned} \tag{7}$$

By using the Usov *ansatz* of the vortex core profile,[14,43] we can use $G = 2\pi M_s pd/|\gamma|$ and $D = (\pi M_s d/|\gamma|)[2 + \ln(R/b)]$, where d is the film thickness, p is the core polarity, R is the system size, and b is the vortex core radius.[35] The derived equations of motion seem to be similar with Eq. (2), because $\dot{\boldsymbol{\xi}} \propto \ddot{\mathbf{X}}$ in a steady-state motion. However, Eq. (2) does not consider the energy variation by the deformation; thus, the force is determined by only the core position, $\mathbf{X}$. Note that Eqs. (3) and (6) can be applicable to other topological solitons in two-dimensional systems, such as magnetic skyrmions, with appropriate G, D, and U.

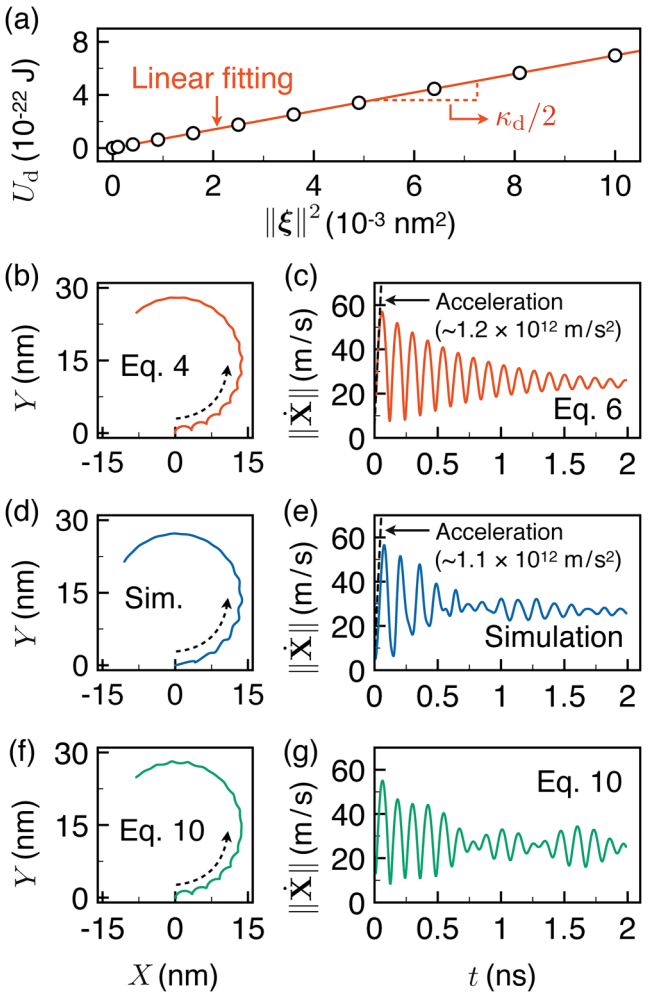

FIG. 2. (a) Deformation energy, U_d, as a function of $\|\xi\|^2$ (symbols) with the linear fit (red line). (b) Trajectory of the vortex core for 2 ns obtained by solving Eq. (6) with $\kappa_d = 0.14\,\mathrm{J/m^2}$. The motion is excited by an in-plane 2 mT magnetic field. (c) Time evolution of the core speed, $\|\dot{\mathbf{X}}\|$, during the motion in (b). (d) Core trajectory obtained from a micromagnetic simulation. (e) Time evolution of $\|\dot{\mathbf{X}}\|$ during the motion presented in (d). The dashed lines in (c) and (e) indicate the initial acceleration. (f) Core trajectory calculated from the hand-waving model [Eq. (10)] in which the interaction with spin-wave modes are simply considered. (g) Time evolution of $\|\dot{\mathbf{X}}\|$ during the motion presented in (f).

Consider now the total magnetic energy, $U(\mathbf{X}, \boldsymbol{\xi})$, which can be expressed to lowest order as $U = U_0 + U_p(\mathbf{X}) + U_d(\boldsymbol{\xi})$, where U_0 is the ground state energy, and $U_p(\mathbf{X})$ and $U_d(\boldsymbol{\xi})$ are the potential and deformation-induced energies, respectively. In a thin film disk, $U_p(\mathbf{X}) \approx (\kappa_p/2)\|\mathbf{X}\|^2$ to lowest order in $\mathbf{X}$, where κ_p is a stiffness coefficient.[14,44,45] We can also write to lowest order in $\boldsymbol{\xi}$,

$$U_d(\boldsymbol{\xi}) \approx \frac{1}{2}\kappa_d\|\boldsymbol{\xi}\|^2, \tag{8}$$

under a sufficiently small deformation. In this work, we determine the parameter κ_d numerically from micromagnetic calculations, because both exchange and dipolar interactions should be considered and, unfortunately, we do not have an appropriate model for the magnetostatic energy calculation yet. As an example, here we consider a cylindrical dot with a diameter of $2R = 512$ nm and a thickness of $d = 20$ nm. We use magnetic parameters corresponding to permalloy, where the exchange constant is taken to be $A_{ex} = 10$ pJ/m, $M_s = 0.8$ MA/m, and $\alpha = 0.013$. We consider small deformations of the order $\|\boldsymbol{\xi}\| \leq 0.1$ nm. From the initial vortex state, which is found from energy minimization, we obtain the deformed configuration using Eq. (3) [see Fig. 1(a)] and then calculate both the exchange and magnetostatic energies. U_d is plotted in Fig. 2(a) as a function of $\|\boldsymbol{\xi}\|^2$, where the slope corresponds to $\kappa_d/2$. For this set of parameters, $\kappa_d \approx 0.14\,\mathrm{J/m^2}$. Note that, despite of the singularity of the deformation *ansatz* at the center, κ_d and U_d have finite values because $\delta\phi$ has a period of 2π.

III. TRANSIENT INERTIAL DYNAMICS

By using the fitted value of κ_d, we can determine the inertial motion of the core under a static in-plane magnetic field, $\|\mathbf{B}\| = 2$ mT. For this, we include an additional Zeeman term, $U_B(\mathbf{X}) = \mu(\hat{\mathbf{z}} \times \mathbf{B}) \cdot \mathbf{X}$, where $\mu \approx (2/3)M_s/R$.[35] The numerically calculated core trajectory and velocity using Eq. (6) with $\kappa_d = 0.14\,\mathrm{J/m^2}$ are presented in Figs. 2(b) and 2(c), respectively. After applying the field, the core exhibits additional oscillatory motion on top of the usual gyration, which also results in oscillations in the speed $\|\dot{\mathbf{X}}\|$. By assuming a negligibly small damping, $\alpha = 0$, the frequency is obtained analytically from Eq. (6),

$$f \approx \frac{G(\kappa_p + \kappa_d) \pm \sqrt{G^2(\kappa_p - \kappa_d)^2 + 4D^2\kappa_p\kappa_d}}{4\pi(G^2 - D^2)}. \tag{9}$$

In our case, the calculated frequencies are $f = 305$ MHz and -8.0 GHz, which corresponds with the frequencies of the counterclockwise (CCW) gyrotropic motion and the clockwise (CW) small oscillation, respectively.

We compare the calculation result with the micromagnetic simulation result. We conduct a micromagnetic simulation using the MuMax3 code[46] with same geometry and material parameters stated above. The initial vortex state has clockwise chirality and upward core, and the system is uniformly discretized by a unit cell of $0.5 \times 0.5 \times 20\,\mathrm{nm^3}$. The simulation result is presented in Figs. 2(d) and 2(e), which is in good agreement with the results from Eq. (6). The frequencies of the core gyration and the small oscillation obtained from the simulation are ~320 MHz and

~7 GHz, respectively, which are quantitatively comparable with the frequencies calculated from Eq. (9).

The micromagnetic simulations also show an additional modulation in the transient response, which can be seen as an oscillation in the envelope of the core velocity in Fig. 2(e), a feature that is absent in the model prediction as given in Fig. 2(c). We can explain this additional modulation by taking into account the excitation of higher-order spin-wave modes that are excited as a result of the core dynamics. Consider the following hand-waving model in which we assume that the overall displacement of the core can be simply given by

$$X_{\rm tot} = X + X_{\rm cw} + X_{\rm ccw}, \tag{10}$$

where

$$\begin{aligned} X_{\rm cw}(t) + iY_{\rm cw}(t) &= R_{\rm sw}\exp[-2\pi i\nu_{\rm cw}(t-\tau)],\\ X_{\rm ccw}(t) + iY_{\rm ccw}(t) &= R_{\rm sw}\exp[2\pi i\nu_{\rm ccw}(t-\tau)], \end{aligned} \tag{11}$$

are the additional core motion induced by clockwise (CW) and counterclockwise (CCW) directional azimuthal spin-wave modes, respectively. $R_{\rm sw}$ characterizes the spin-wave amplitude and τ is a time delay, which accounts for the phase of the spin-wave mode. Here, we assume that $R_{\rm sw}$ and τ are same for both CW and CCW spin-wave modes and they are not influenced by the core position and deformation to simplify the calculation. In our system, the first-order azimuthal spin-wave frequencies for CW and CCW propagation directions are found to be $\nu_{\rm cw} = 6.4$ GHz and $\nu_{\rm ccw} = 7.7$ GHz, respectively. With arbitrary parameters, $R_{\rm sw} = 0.1$ nm and $\tau = 0$ ns, we obtain the core trajectory and speed as shown in Figs. 2(f) and 2(g), respectively. The results show that slow modulation with beating pattern can appear in the evolution of the core speed similar with the simulation [Fig. 2(e)].

By considering a linear steady-state motion of the core, the relation between the deformation energy and the core velocity, $U_{\rm d} = \frac{1}{2}\mathcal{M}\|\dot{\mathbf{X}}\|^2$, can be obtained from Eqs. (6) and (8), where

$$\mathcal{M} \equiv \frac{D^2}{\kappa_{\rm d}}, \tag{12}$$

which can be regarded as an effective inertial mass under small deformations. In the case of $2R = 512$ nm and $d = 20$ nm of a NiFe cylindrical dot, for example, the mass is found to be $\mathcal{M}_{\rm NiFe} \approx 1.4\times10^{-23}$ kg, which is similar to the values for domain walls obtained from experiments.[47]

The acceleration of the core can be calculated from $\ddot{\mathbf{X}} = \mathbf{F}/\mathcal{M}$, where $\mathbf{F}$ is a force exerted on the core. If $\|\mathbf{B}\| = 2$ mT is applied on a stable vortex core, the acceleration will be $\|\ddot{\mathbf{X}}\| = \|\mathbf{F}_{\rm B}\|/\mathcal{M}_{\rm NiFe} \approx 1.2\times10^{12}$ m/s^2, where $\mathbf{F}_{\rm B} = -\mu|\mathbf{B}|\pi R^2 d$ is the force from the in-plane field.[35] As shown in Figs. 2(c) and 2(e) (dashed line), the calculated acceleration value is in a good agreement with those obtained from the simulation $\|\ddot{\mathbf{X}}\| \approx 1.1\times10^{12}$ m/s^2.

IV. VELOCITY DEPENDENCE OF INERTIAL MASS

We now turn our attention to the inertial mass under large deformations beyond the range for which Eqs. (8) and (12) are valid. In this limit, the deformation model [Eq. (3)] cannot be used to calculate $U_{\rm d}$ since the magnetic energy is overestimated particularly at the core center, because the model cannot describe deformation of the vortex core properly [see Fig. 3]. Therefore, we extract the inertial mass from micromagnetic simulations at stable deformed-vortex configurations under a static-uniform in-plane electric current.[48] The equations of motion with an adiabatic spin-transfer torque are given by

$$\mathbf{G}\times\left(\dot{\mathbf{X}} - \mathbf{u} - \alpha\dot{\boldsymbol{\xi}}\right) + \overleftrightarrow{D}\cdot\left(\alpha\dot{\mathbf{X}} + \dot{\boldsymbol{\xi}}\right) = -\frac{\partial U}{\partial \mathbf{X}}, \tag{13a}$$

$$\mathbf{G}\times\left(\dot{\boldsymbol{\xi}} + \alpha\dot{\mathbf{X}}\right) + \overleftrightarrow{D}\cdot\left(\alpha\dot{\boldsymbol{\xi}} - \dot{\mathbf{X}} + \mathbf{u}\right) = -\frac{\partial U}{\partial \boldsymbol{\xi}}, \tag{13b}$$

where $\mathbf{u} = \mathbf{J}Pg\mu_{\rm B}/(2eM_{\rm s})$ represents an effective spin-drift velocity that is proportional to the applied current density $\mathbf{J}$ and spin polarization $P = 0.5$. Under applied currents, deformed core configurations can be obtained without any core motion, since $\mathbf{u}$ acts as the core-motion velocity $-\dot{\mathbf{X}}$ when only adiabatic term is considered in the limit $\alpha \ll 1$. In the immobile state, we obtain the core displacement from the center of the disk, $\|\mathbf{X}\|$, and the total magnetic energy, U, as a function of $\|\mathbf{u}\|$ [black lines in Figs. 4(a) and 4(b)]; both $\|\mathbf{X}\|$ and U increase with an increasing $\|\mathbf{u}\|$ up to the critical value at ~280 m/s above which the stationary state changes due to reversal of the vortex core. From the $\|\mathbf{X}\|$ and U obtained, we dissociate the deformation energy, $U_{\rm d} = U - U_0 - (\kappa_{\rm p}/2)\|\mathbf{X}\|^2$ [red line in Fig. 4(b)], then calculate the effective inertial mass from $\mathcal{M} = 2U_{\rm d}/\|\mathbf{u}\|^2$. Here we assume that $\mathcal{M} \to D^2/\kappa_{\rm d}$ when $\|\mathbf{u}\| \to 0$ to find the reasonable $\kappa_{\rm p}$ value. The obtained $\mathcal{M}$ is plotted in Fig. 4(c) as a function of $\|\mathbf{u}\|$ (red line). The result shows that the

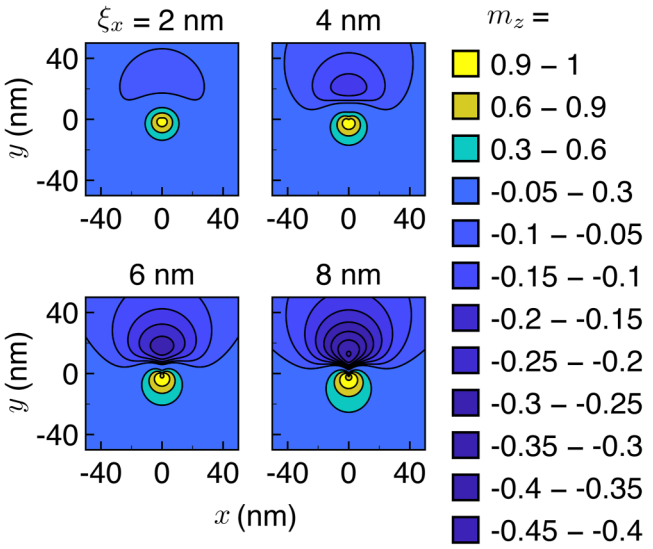

FIG. 3. Contour lines of the z-component of the local magnetization, m_z, of deformed-vortex-core configurations calculated from the analytic deformation model [Eq. (3)] with different deformation parameters, ξ_x.

mass depends on the velocity; $\mathcal{M}$ gradually increases with an increasing $\|\mathbf{u}\|$ from D^2/κ_d, in particular, $\mathcal{M}$ increases drastically near the critical velocity, ~280 m/s. Because $\|\mathbf{u}\| \approx \|\dot{\mathbf{X}}\|$ in this case, the result implies that the effective inertial mass increases with an increasing the core velocity.

The initial core acceleration, $\|\ddot{\mathbf{X}}\|$, can be obtained using micromagnetic simulations in which an in-plane field, $\|\mathbf{B}\| = 2$ mT, is applied to different stationary deformed configurations under $\|\mathbf{u}\|$. We plot the time evolution of the velocity in Fig. 4(d) and present their initial acceleration as a function of $\|\mathbf{u}\|$ in Fig. 4(e). The result shows that the acceleration reduces with increasing $\|\mathbf{u}\|$ as expected from the increase in mass. By using the obtained $\|\ddot{\mathbf{X}}\|$, we calculate the inertial mass from $\mathcal{M} = \|\mathbf{F}_B\|/\|\ddot{\mathbf{X}}\|$ and plot it in Fig. 4(c) using blue circles, which is in good agreement with the mass calculated for the deformation energy. This result shows that the effective mass depends on the core velocity and the core deformation.

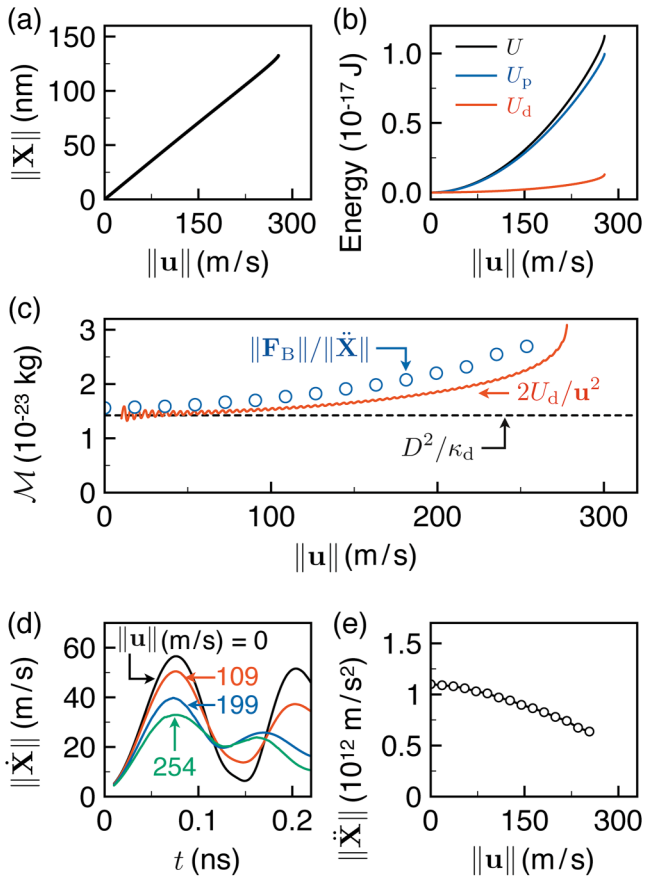

FIG. 4. (a) Core position displacement, $\|\mathbf{X}\|$, as a function of an effective spin-current drift velocity, $\|\mathbf{u}\|$. (b) Total magnetic energy, U, the potential energy, U_p, and the deformation energy, U_d, as a function of $\|\mathbf{u}\|$. (c) Inertial mass of the vortex, $\mathcal{M}$, as a function of $\|\mathbf{u}\|$ obtained from $\mathcal{M} = 2U_d/\mathbf{u}^2$ (red line). The black dashed line indicates the mass at rest calculated from Eq. (12). The blue circles are $\mathcal{M}$ obtained from the acceleration, $\|\ddot{\mathbf{X}}\|$, shown in (e). (d) Time evolution of $\|\dot{\mathbf{X}}\|$ for different $\|\mathbf{u}\|$. (e) The initial acceleration, $\|\ddot{\mathbf{X}}\|$, obtained from (d).

V. INERTIAL EFFECTS IN CORE REVERSAL

Vortex core reversal is analogous to Walker breakdown in domain walls, whereby the deformed equilibrium micromagnetic profile moving at a constant velocity no longer satisfies the Landau–Lifshitz equation. To probe this limit with the deformation model, we need to compute the deformation energy $U_d(\|\boldsymbol{\xi}\|)$ to the point at which the restoring force $\|\partial_{\boldsymbol{\xi}} U_d\|$ vanishes, by analogy with Walker breakdown. Because of the limit of the deformation model under a large deformation, we achieve this by using micromagnetic simulations with adiabatic spin-transfer torques as follows. From Eq. (13b), we obtain a relation $Du_x = -\partial U_d/\partial \xi_x$ at the stationary deformed state under an in-plane current flowing along x, where $\dot{X} = \dot{Y} = \dot{\xi}_x = \dot{\xi}_y = 0$. D, u_x, and U_d values can be taken from the simulations, thus we can numerically obtain ξ_x by assuming $\partial U_d = \Delta U_d$ and $\partial \xi_x = \Delta \xi_x$.

The computed deformation energy, U_d, and its derivative, $\|\partial_{\boldsymbol{\xi}} U_d\|$, are shown as a function of $\|\boldsymbol{\xi}\|$ in Figs. 5(a) and 5(b), respectively, with black solid lines. As these figures show, the quadratic approximation in Eq. (8) is insufficient when $\|\boldsymbol{\xi}\|$ becomes large. Moreover, the slope of $\|\partial_{\boldsymbol{\xi}} U_d\|$ almost vanishes at the maximum value, $F_{d,0}$.

With our method, we cannot obtain the energy profile when $\|\boldsymbol{\xi}\| > \|\boldsymbol{\xi}_0\|$. However, from the obtained data, U_d and $\|\partial_{\boldsymbol{\xi}} U_d\|$, we can infer that U_d increases with an increasing $\|\boldsymbol{\xi}\|$ up to the critical energy barrier, $U_{d,max}$, for the core switching, but $\|\partial_{\boldsymbol{\xi}} U_d\|$ decreases from $F_{d,0}$, which results in a spontaneous core switching when a driving force is applied continuously.

To account for this behavior, we can use a higher-order polynomial expansion in $\|\boldsymbol{\xi}\|$,

$$U_d = \frac{1}{2}\kappa_d \|\boldsymbol{\xi}\|^2 + C_1 \|\boldsymbol{\xi}\|^3 + C_2 \|\boldsymbol{\xi}\|^4, \tag{14}$$

which accounts for deformations up to $\|\boldsymbol{\xi}_0\|$, i.e., the point at which the restoring force attains its maximum, $F_{d,max} = 3.9 \times 10^{-10}$ N. With the fitted values of $C_1 = -2.4 \times 10^6$ J/m^3 and $C_2 = -2.6 \times 10^{14}$ J/m^4, Eq. (14) provides a good description of the potential energy profile [Fig. 5(a)] and restoring force [Fig. 5(b)] up to $F_{d,max}$, and shows the expected characteristics stated above.

This model explains the maximum core velocity attained before core switching. If the core motion is carefully excited with sufficiently small $\|\dot{\boldsymbol{\xi}}\|$, U_d increases following Eq. (14) and the core switching occurs when $U_d = U_{d,max}$. During the dynamics, the core velocity is approximately $\|\dot{\mathbf{X}}\| \approx \|\partial_{\boldsymbol{\xi}} U_d\|/D$ if $\alpha \ll 1$; therefore, generally the velocity does not exceed the maximum value, $F_{d,0}/D$.

Since the restoring force attains a maximum value at $\|\boldsymbol{\xi}_0\|$ while the deformation energy continues to increase for $\|\boldsymbol{\xi}\| > \|\boldsymbol{\xi}_0\|$, it suggests that core reversal is related to a critical deformation being reached, rather than a critical velocity. To illustrate this, we consider the resonant excitation of the vortex dynamics by a rotating field, $\mathbf{B}_{CCW} = (B_0 \cos \omega t, B_0 \sin \omega t, 0)$, where $B_0 = 1.3$ mT and $\omega/2\pi = 320$ MHz with the same micromagnetic parameters considered above. When the field is applied continuously, the core reaches the maximum velocity at ~11.9 ns, after which the velocity decreases and the core reverses at ~12.6 ns, as shown by the solid black line in Fig. 5(c). However, if the field is switched off just after the nominal

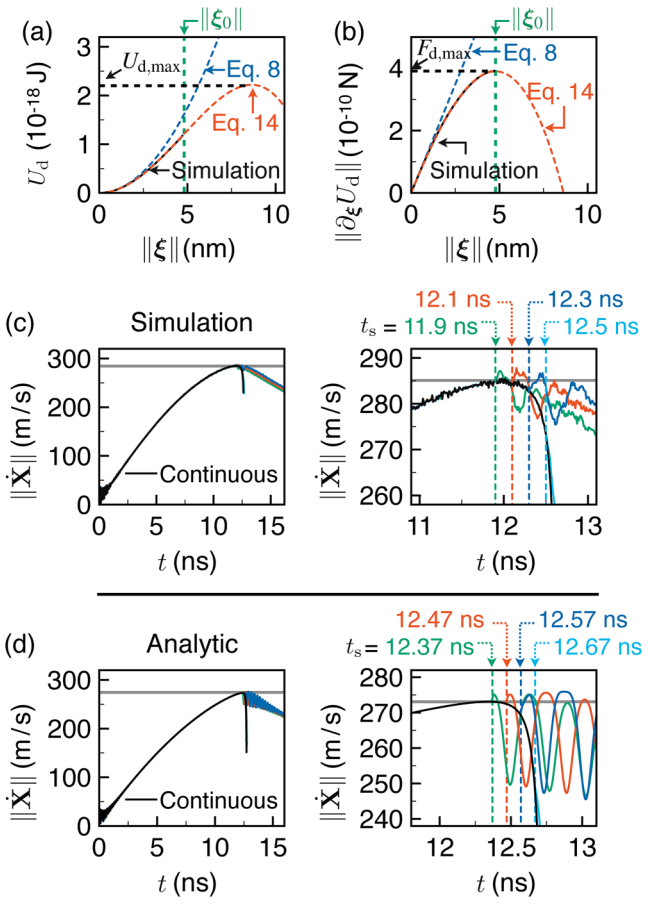

FIG. 5. (a) Deformation energy, U_d, as a function of the deformation amplitude, $\|\xi\|$ (black line). The blue dashed line is Eq. (8) and the red dashed line is Eq. (14). (b) Derivative of the deformation energy, $\|\partial_\xi U_d\|$, as a function of $\|\xi\|$. (c) $\|\dot{\mathbf{X}}\|$ during the resonant excitation obtained from micromagnetic simulations. The black line is the result from a continuous excitation up to the core reversal and the gray line indicates the maximum core velocity. The green, red, blue, and light blue lines indicate the velocity when the driving field is turned off at t_s as shown in the right panel, which shows a zoom on the region around the maximum core velocity. (d) as in (c) but obtained by solving Eq. (6) with Eq. (14).

maximum velocity is reached, core reversal *does not* take place [green, red, and blue lines in Fig. 5(c)]. In those cases, the core velocity can even exceed the nominal maximum velocity instantaneously just after turning off the field, because of a relatively large $\dot{\xi}$ from the deformation dynamics. Core reversal occurs if the field is turned off too late [light blue line in Fig. 5(c)]. These phenomena can be reproduced with the deformation model by solving Eq. (6) with Eq. (14), as shown in Fig. 5(d). Besides providing an accurate description of the dynamics up to the core reversal transition, the result illustrates the importance of inertial effects where core reversal can be inhibited, even though the velocity maximum has been attained, if the driving force is switched off sufficiently early.

VI. DISCUSSION AND CONCLUDING REMARKS

We have discussed in some depth how the inertial dynamics of magnetic vortices can be understood in terms of the Döring mechanism, which has been more extensively studied for domain wall dynamics. We can show indeed that our proposed *ansatz* [Eq. (3)] gives rise to the standard one-dimensional model for domain wall dynamics. This model involves two dynamical variables: the wall position, $q(t)$, and the internal wall angle, $\varphi(t)$, which plays the role of the deformation. The equations of motion, as established by Slonczewski, Walker, and Schryer, are given by

$$\begin{aligned} \alpha\frac{\dot{q}}{\Delta}+\dot{\varphi} &= -\frac{\gamma}{2M_s}\frac{\partial U}{\partial q},\\ -\frac{\dot{q}}{\Delta}+\alpha\dot{\varphi} &= -\frac{\gamma}{2M_s\Delta}\frac{\partial U}{\partial \varphi}, \end{aligned} \tag{15}$$

where Δ is the characteristic wall width and U represents the potential energy seen by the wall. Consider a perpendicularly magnetized system, where the static magnetization profile of the domain wall, $\mathbf{m}_0(x) = (\cos\phi_0 \sin\theta_0,\ \sin\phi_0 \sin\theta_0,\ \cos\theta_0)$, can be written in terms of the polar θ and azimuthal ϕ angles as

$$\begin{aligned} \theta_0 &= 2\tan^{-1}\left[\exp\left(\frac{x-q}{\Delta}\right)\right],\\ \phi_0 &= \text{const.}, \end{aligned} \tag{16}$$

respectively. The precise value of ϕ_0 determines whether it is a Bloch or a Néel form. We follow our prescription by elevating $q(t)$ to a dynamical variable and by including the deformation, parametrized here by $\xi_x(t)$,

$$\begin{aligned} \theta &= \theta_0 - (\xi_x(t)\cdot\nabla\phi_0)\sin\theta_0 = \theta_0[x-q(t)],\\ \phi &= \phi_0 + \frac{1}{\sin\theta_0}(\xi_x(t)\cdot\nabla\theta_0) = \phi_0 + \frac{\xi_x(t)}{\Delta}. \end{aligned} \tag{17}$$

From the Lagrangian and Rayleigh dissipation function for the Gilbert damping [Eq. (5)], we can obtain the Euler–Lagrange equations with Eq. (17), which give the equations of motion,

$$\begin{aligned} \alpha\frac{\dot{q}}{\Delta}+\frac{\dot{\xi}_x}{\Delta} &= -\frac{\gamma}{2M_s}\frac{\partial U}{\partial q},\\ -\frac{\dot{q}}{\Delta}+\alpha\frac{\dot{\xi}_x}{\Delta} &= -\frac{\gamma}{2M_s}\frac{\partial U}{\partial \xi_x}. \end{aligned} \tag{18}$$

By making the identification, $\varphi \equiv \xi_x/\Delta$, we recover the equations of motion in Eq. (15). This simple derivation shows that we can recover other well-established results with our model with no modification. Note that, here we do not consider the variation of Δ,[49,50] because the deformation ansatz, Eq. (17), and the equations of motion, Eq. (18), cannot describe the domain wall width change during the motion.

As we noted in the introduction, previous theoretical works have sought to interpret the inertial mass of vortices in terms of coupling to spin waves.[16,27–30] In light of our results shown in

Fig. 2, we suggest that coupling to spin waves can result in higher-order effects in the inertial dynamics but do not constitute the primary mechanism, which we find to be core deformation. The coupling to spin waves, such as azimuthal spin-wave modes in a dot, results in a GHz-frequency modulation of the inertial dynamics but does not fully account for the cycloidal-type motion arising from the core deformations. Because core deformation is in part tied to a potential energy term related to the vortex helicity, i.e., the cost in dipolar energy as a result of deviations from the Bloch-like configuration of the magnetization, we hypothesize that such features may have been overlooked in earlier work where only easy-plane anisotropies were considered in addition to the exchange interaction in atomistic models. Indeed, the absence of a helicity dependence in the domain wall case amounts to $U(\varphi) = \text{const.}$, resulting in the absence of a domain wall mass. Moreover, a more recent study in which full dipolar interactions are taken into account shows that coupling to spin waves only accounts for part of the inertial dynamics observed.[30]

In summary, we have developed a deformation model based on the Döring mechanism, which describes the inertial dynamics of magnetic vortices and is valid up to the core reversal transition. It provides a straightforward generalization of the Thiele equation through the inclusion of additional deformation amplitudes, which are dynamical variables. The method is general and can be extended to describe other two-dimensional topological magnetic solitons, such as skyrmions. We anticipate that further generalization to N dimensions is possible, thereby providing a standard prescription for describing the inertial effects of topological magnetic solitons.

ACKNOWLEDGMENTS

This work was partially supported by the Agence Nationale de la Recherche under Contract No. ANR-17-CE24-0008 (CHIPMuNCS).

DATA AVAILABILITY

The data that support the findings of this study are available from the corresponding author upon reasonable request.

REFERENCES

[1]F. Bloch, "Zur theorie des austauschproblems und der remanenzerscheinung der ferromagnetika," Z. Phys. A **74**, 295–335 (1932).
[2]A. Hubert and R. Schäfer, *Magnetic Domains: The Analysis of Magnetic Microstructures* (Springer-Verlag, Berlin, 1998).
[3]M. E. Gouvêa, G. M. Wysin, A. R. Bishop, and F. G. Mertens, "Vortices in the classical two-dimensional anisotropic Heisenberg model," Phys. Rev. B **39**, 11840–11849 (1989).
[4]N. Papanicolaou and T. N. Tomaras, "Dynamics of magnetic vortices," Nuclear Phys. **360**, 425–462 (1991).
[5]R. P. Cowburn, D. K. Koltsov, A. O. Adeyeye, M. E. Welland, and D. M. Tricker, "Single-domain circular nanomagnets," Phys. Rev. Lett. **83**, 1042–1045 (1999).
[6]T. Shinjo, T. Okuno, R. Hassdorf, K. Shigeto, and T. Ono, "Magnetic vortex core observation in circular dots of permalloy," Science **289**, 930–932 (2000).
[7]A. Bogdanov and A. Hubert, "Thermodynamically stable magnetic vortex states in magnetic crystals," J. Magn. Magn. Mater. **138**, 255–269 (1994).
[8]A. N. Bogdanov and D. A. Yablonskii, "Thermodynamically stable "vortices" in magnetically ordered crystals. The mixed state of magnets," J. Exp. Theor. Phys. **68**, 101–103 (1989), see http://www.jetp.ac.ru/cgi-bin/e/index/e/68/1/p101?a=list.
[9]A. A. Thiele, "Steady-state motion of magnetic domains," Phys. Rev. Lett. **30**, 230–233 (1973).
[10]D. L. Huber, "Dynamics of spin vortices in two-dimensional planar magnets," Phys. Rev. B **26**, 3758–3765 (1982).
[11]W. Döring, "Über die trägheit der Wände zwischen weißschen bezirken," Z. Naturforsch. A **3a**, 373–379 (1948).
[12]J. C. Slonczewski, "Dynamics of magnetic domain walls," AIP Conf. Proc. **5**, 170–174 (1972).
[13]N. L. Schryer and L. R. Walker, "The motion of 180° domain walls in uniform dc magnetic fields," J. Appl. Phys. **45**, 5406–5421 (1974).
[14]K. Y. Guslienko, B. A. Ivanov, V. Novosad, Y. Otani, H. Shima, and K. Fukamichi, "Eigenfrequencies of vortex state excitations in magnetic submicron-size disks," J. Appl. Phys. **91**, 8037–8039 (2002).
[15]K. Everschor, M. Garst, B. Binz, F. Jonietz, S. Mühlbauer, C. Pfleiderer, and A. Rosch, "Rotating skyrmion lattices by spin torques and field or temperature gradients," Phys. Rev. B **86**, 054432 (2012).
[16]B. A. Ivanov and V. A. Stephanovich, "Two-dimensional soliton dynamics in ferromagnets," Phys. Lett. A **141**, 89–94 (1989).
[17]G. M. Wysin, "Magnetic vortex mass in two-dimensional easy-plane magnets," Phys. Rev. B **54**, 15156–15162 (1996).
[18]V. Novosad, F. Y. Fradin, P. E. Roy, K. S. Buchanan, K. Y. Guslienko, and S. D. Bader, "Magnetic vortex resonance in patterned ferromagnetic dots," Phys. Rev. B **72**, 024455 (2005).
[19]B. Van Waeyenberge, A. Puzic, H. Stoll, K. W. Chou, T. Tyliszczak, R. Hertel, M. Fähnle, H. Brückl, K. Rott, G. Reiss, I. Neudecker, D. Weiss, C. H. Back, and G. Schütz, "Magnetic vortex core reversal by excitation with short bursts of an alternating field," Nature **444**, 461–464 (2006).
[20]A. Vansteenkiste, K. W. Chou, M. Weigand, M. Curcic, V. Sackmann, H. Stoll, T. Tyliszczak, G. Woltersdorf, C. H. Back, G. Schütz, and B. Van Waeyenberge, "X-ray imaging of the dynamic magnetic vortex core deformation," Nat. Phys. **5**, 332–334 (2009).
[21]R. E. Troncoso and Á. S. Núñez, "Brownian motion of massive skyrmions in magnetic thin films," Ann. Phys. (NY) **351**, 850–856 (2014).
[22]M. Buess, R. Höllinger, T. Haug, K. Perzlmaier, U. Krey, D. Pescia, M. R. Scheinfein, D. Weiss, and C. H. Back, "Fourier transform imaging of spin vortex eigenmodes," Phys. Rev. Lett. **93**, 077207 (2004).
[23]J. V. Kim, F. Garcia-Sanchez, J. Sampaio, C. Moreau-Luchaire, V. Cros, and A. Fert, "Breathing modes of confined skyrmions in ultrathin magnetic dots," Phys. Rev. B **90**, 064410 (2014).
[24]J. Ding, G. N. Kakazei, X. Liu, K. Y. Guslienko, and A. O. Adeyeye, "Higher order vortex gyrotropic modes in circular ferromagnetic nanodots," Sci. Rep. **4**, 4796 (2014).
[25]K. Y. Guslienko, "Magnetic vortex state stability reversal and dynamics in restricted geometries," J. Nanosci. Nanotechnol. **8**, 2745–2760 (2008).
[26]K. Y. Guslienko, "Magnetic vortices and skyrmions," J. Magn. **24**, 549–567 (2019).
[27]B. A. Ivanov, H. J. Schnitzer, F. G. Mertens, and G. M. Wysin, "Magnon modes and magnon-vortex scattering in two-dimensional easy-plane ferromagnets," Phys. Rev. B **58**, 8464–8474 (1998).
[28]A. S. Kovalev, F. G. Mertens, and H. J. Schnitzer, "Cycloidal vortex motion in easy-plane ferromagnets due to interaction with spin waves," Eur. Phys. J. B **33**, 133–145 (2003).
[29]J. P. Zagorodny, Y. Gaididei, D. D. Sheka, J.-G. Caputo, and F. G. Mertens, "Importance of the internal shape mode in magnetic vortex dynamics," Phys. Rev. Lett. **93**, 167201 (2004).
[30]K. Y. Guslienko, G. N. Kakazei, J. Ding, X. M. Liu, and A. O. Adeyeye, "Giant moving vortex mass in thick magnetic nanodots," Sci. Rep. **5**, 13881 (2015).
[31]A. R. Völkel, G. M. Wysin, F. G. Mertens, A. R. Bishop, and H. J. Schnitzer, "Collective-variable approach to the dynamics of nonlinear magnetic excitations with application to vortices," Phys. Rev. B **50**, 12711–12720 (1994).

[32]F. G. Mertens, H. J. Schnitzer, and A. R. Bishop, "Hierarchy of equations of motion for nonlinear coherent excitations applied to magnetic vortices," Phys. Rev. B **56**, 2510–2520 (1997).
[33]D. D. Sheka, B. A. Ivanov, and F. G. Mertens, "Internal modes and magnon scattering on topological solitons in two-dimensional easy-axis ferromagnets," Phys. Rev. B **64**, 024432 (2001).
[34]D. D. Sheka, C. Schuster, B. A. Ivanov, and F. G. Mertens, "Dynamics of topological solitons in two-dimensional ferromagnets," Eur. Phys. J. B **50**, 393–402 (2006).
[35]K. Y. Guslienko, "Low-frequency vortex dynamic susceptibility and relaxation in mesoscopic ferromagnetic dots," Appl. Phys. Lett. **89**, 022510 (2006).
[36]R. Hertel and C. M. Schneider, "Exchange explosions: Magnetization dynamics during vortex–antivortex annihilation," Phys. Rev. Lett. **97**, 177202 (2006).
[37]K. Yamada, S. Kasai, Y. Nakatani, K. Kobayashi, H. Kohno, A. Thiaville, and T. Ono, "Electrical switching of the vortex core in a magnetic disk," Nat. Mater. **6**, 270–273 (2007).
[38]K. Y. Guslienko, K.-S. Lee, and S.-K. Kim, "Dynamic origin of vortex core switching in soft magnetic nanodots," Phys. Rev. Lett. **100**, 027203 (2008).
[39]U. Ritzmann, S. von Malottki, J.-V. Kim, S. Heinze, J. Sinova, and B. Dupé, "Trochoidal motion and pair generation in skyrmion and antiskyrmion dynamics under spin–orbit torques," Nat. Electron. **1**, 451–457 (2018).
[40]A. Thiaville and Y. Nakatani, "Domain-wall dynamics in nanowires and nanostrips," in *Spin Dynamics in Confined Magnetic Structures III*, edited by B. Hillebrands and A. Thiaville (Springer-Verlag, Berlin, 2006), pp. 161–205.
[41]J.-V. Kim, "Spin-torque oscillators," in *Solid State Physics*, edited by R. E. Camley and R. L. Stamps (Academic Press, San Diego, 2012), Vol. 63, Chap. 4, pp. 217–294.
[42]K. L. Metlov, "Vortex mechanics in planar nanomagnets," Phys. Rev. B **88**, 014427 (2013).
[43]N. A. Usov and S. E. Peschany, "Magnetization curling in a fine cylindrical particle," J. Magn. Magn. Mater. **118**, L290–L294 (1993).
[44]K. Y. Guslienko and K. L. Metlov, "Evolution and stability of a magnetic vortex in a small cylindrical ferromagnetic particle under applied field," Phys. Rev. B **63**, 100403(R) (2001).
[45]K. Y. Guslienko, X. F. Han, D. J. Keavney, R. Divan, and S. D. Bader, "Magnetic vortex core dynamics in cylindrical ferromagnetic dots," Phys. Rev. Lett. **96**, 067205 (2006).
[46]A. Vansteenkiste, J. Leliaert, M. Dvornik, M. Helsen, F. Garcia-Sanchez, and B. Van Waeyenberge, "The design and verification of MuMax3," AIP Adv. **4**, 107133 (2014).
[47]E. Saitoh, H. Miyajima, T. Yamaoka, and G. Tatara, "Current-induced resonance and mass determination of a single magnetic domain wall," Nature **432**, 203–206 (2004).
[48]V. P. Kravchuk, D. D. Sheka, F. G. Mertens, and Y. Gaididei, "Off-centred immobile magnetic vortex under influence of spin-transfer torque," J. Phys. D Appl. Phys. **44**, 285001 (2011).
[49]A. Thiaville, J. M. García, and J. Miltat, "Domain wall dynamics in nanowires," J. Magn. Magn. Mater. **242–245**, 1061–1063 (2002).
[50]L. Sánchez-Tejerina, V. Puliafito, P. Khalili Amiri, M. Carpentieri, and G. Finocchio, "Dynamics of domain-wall motion driven by spin–orbit torque in antiferromagnets," Phys. Rev. B **101**, 014433 (2020).